Laser and Particle Beams (2008), *26*, 147–155. Printed in the USA.

doi:10.1017/S0263034608000177

Quasi-monoenergetic electron beams generated from 7 TW laser pulses in N_2 and He gas targets

Z.L. CHEN,[1] C. UNICK,[1] N. VAFAEI-NAJAFABADI,[1] Y.Y. TSUI,[1] R. FEDOSEJEVS,[1] N. NASERI,[2] P.-E. MASSON-LABORDE,[2] AND W. ROZMUS[2]

[1]Department of Electrical and Computer Engineering, University of Alberta, Edmonton, Alberta, Canada
[2]Department of Physics, University of Alberta, Edmonton, Alberta, Canada

(RECEIVED 24 December 2007; ACCEPTED 3 March 2008)

Abstract

Quasi-monoenergetic electron beams of energies 12 MeV to over 200 MeV are generated from both nitrogen and helium gas targets with 7TW laser pulses. Typically nitrogen gas interactions lead to electron bunches in the range of 12 to 50 MeV varying from shot to shot. Helium gas leads to higher energy electron bunches from 25 to 100 MeV. Occasionally exceptionally high energy bunches of electrons up to 200 MeV are observed from nitrogen and helium. Initial full two-dimensional simulations indicate the production of 20–30 MeV electron energy bunches for the typical interaction conditions as the electrons are injected from wave breaking in the plasma wake behind the laser pulse and injected into the strong electric field gradient propagating with the optical pulse. This is consistent with the experimental observations from the majority of shots. Pulse compression during propagation in the high density plasma does not allow the threshold conditions for the full bubble regime to be reached. However, the electric acceleration field in the wakefield cavity is still sufficient to lead to the formation of a bunch of electrons with an energy peak in the range of 20 to 30 MeV. In order to explain the occasional high energy shots most likely a lower density channel created by the laser prepulse may occasionally form a natural low density electron guide channel giving ideal conditions for acceleration over much longer lengths leading to the high energies observed.

Keywords: Gas target; Laser plasma interaction; Monoenergetic electrons; PIC simulation; Wakefield acceleration

INTRODUCTION

Laser electron acceleration (Tajima & Dawson, 1979) is a promising new approach for the development of next generation electron accelerators. GeV electron beam generation has been predicted by multiple simulations (Lifschitz *et al.*, 2005, 2006) and demonstrated in very recent experiments (Leemans *et al.*, 2006). Such laser based accelerators might be expected to replace traditional accelerators in the near future. Recent experiments have demonstrated the generation of high quality monoenergetic electron beams with different energies and fluxes, through the interaction of laser pulses with powers higher than 10 TW with gases of hydrogen or helium (Mangles *et al.*, 2004; Geddes *et al.*, 2004; Faure *et al.*, 2004). Another recent experiment measured the acceleration gradient in the wakefield through a tomographic diagnosis method, which clearly shows the acceleration of 55 MeV electron beams from 5 MeV over a 200 μm interaction distance (Hsieh *et al.*, 2006). It is believed that the monoenergetic electron beams are generated in the wakefield or in cavitation bubbles in the electron density profile created by the laser fields when the plasma density ranges between 3×10^{18} cm^{-3} and 5×10^{19} cm^{-3} and the corresponding wavelength of the plasma waves is on the order of the laser pulse length (Tajima & Dawson, 1979; Mangles *et al.*, 2004; Geddes *et al.*, 2004; Faure *et al.*, 2004). A recent study confirms a possibility of modifying the long laser pulse in underdense plasmas to match the necessary conditions and driving the laser plasma interaction to the laser wakefield acceleration even if the initial laser and plasma parameters are outside the required regime (Hidding *et al.*, 2006). The corresponding experiments show highly collimated, quasi-monoenergetic multi-MeV electron bunches generated by the interaction of tightly focused, 80 fs laser pulses in a high-pressure helium gas jet.

Address correspondence and reprint requests to: Robert Fedosejevs, Department of Electrical and Computer Engineering, ECERF W2-104, University of Alberta, Edmonton, Alberta, Canada T6G 2V4. E-mail: rfed@ece.ualberta.ca

In this paper, we report on measurements of electron generation from relatively high plasma electron densities of 5×10^{19} cm^{-3} and higher leading to bunches of electrons with energies typically ranging from 10 to 50 MeV for nitrogen targets and 25 to 100 MeV for helium targets. Such bunches would be consistent with injection of electrons from plasma oscillations breaking in the tail of the laser pulse and being injected into the wake of the main laser pulse as analyzed in two-dimensional (2D) particle in cell modeling. The exact energy of the resultant electrons depends on the time of release of the electrons from the potential well accompanying the laser pulse, which will vary from shot to shot. In addition, we show that on exceptional shots that quasi-monoenergetic electron beams with energies of over 200 MeV can be generated both from helium and nitrogen gases. These very energetic electron beams have been produced with a laser pulse intensity of approximately 7 TW on the target, much less than laser powers employed in previous experiments (Mangles *et al.*, 2004; Geddes *et al.*, 2004; Faure *et al.*, 2004), which have resulted in quasi-monoenergetic electron bunches over 100 MeV.

EXPERIMENTS

Experiments were carried out using the 10 TW laser beamline at the Canadian Advanced Laser Light Source facility (Ozaki *et al.*, 2006) and the experimental set up is shown in Figure 1. The 800 nm horizontally polarized laser pulses with energies up to 300 mJ were compressed to give 31 fs, 200 mJ pulses on target (~7 TW) and focused by a 150 mm focal length off-axis parabolic mirror in an f/6 cone angle into a 13 μm diameter spot on a supersonic gas jet. The resultant peak vacuum laser intensity is approximately 5×10^{18} Wcm^{-2}. The gas jet was generated by a pulsed supersonic nozzle connected to a gas reservoir with backing pressure adjustable from 100 to 1200 psi. Different gases of helium, nitrogen, and nitrogen mixed with hydrogen were employed in the experiments. The initial gas density profile was characterized with interferometric measurements.

A calibrated magnetic electron spectrometer was used to measure the electron energy spectrum on the laser axis in the forward laser direction, where a Lanex fluorescer screen (Kodak) was mounted after the magnet to record the electron beams. A sandwiched detector consisting of radiochromic film and CR-39 was used to measure the electron angular distributions in the forward laser direction on separate laser shots. It was entirely wrapped by a 20 μm thick aluminum foil to block the scattered laser light. Most ions with energies less than 10 MeV were stopped by the Aluminum foil (confirmed by the signals on CR-39), allowing only energetic electrons and a weak X-ray background to hit the detector and radiochromic film.

RESULTS AND ANALYSIS

In the experiments, we scanned the nozzle location along the laser axis to change the position of the laser focus inside the gas jet density profile. An optimum position to generate the monoenergetic electron beams was found with the laser beam incident on the edge of the gas jet, depending on the specific gas density profile formed in the supersonic gas jet. The gas density profile was measured by the interferometer and shown in Figure 2. The optimum gas pressures for nitrogen and helium to generate the quasi-monoenergetic electron beams in the forward laser direction were about 360 psi and 900 psi in these experiments, respectively. These correspond to electron densities in the interaction region of about 9×10^{19} cm^{-3} for nitrogen while about 5×10^{19} cm^{-3} for helium, assuming the charge states of nitrogen and helium are 5^+ and 2^+ (Fedosejevs *et al.*, 1997), respectively.

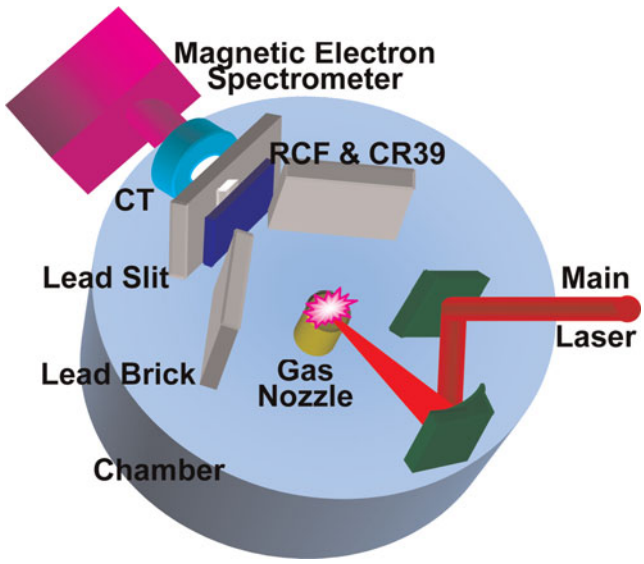

Fig. 1. (Color online) Experimental setup.

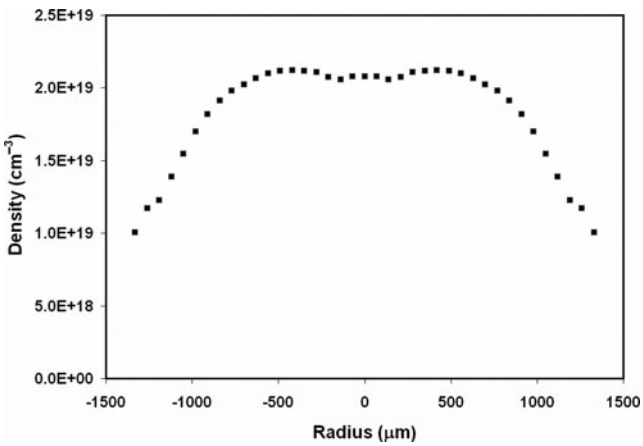

Fig. 2. Typical gas density profile measured by the interferometer when nitrogen gas backing pressure was 1000 psi. The gas jet was generated by a supersonic nozzle which was connected to the gas reservoir with its pressure adjustable from 100 to 1200 psi. The profile shows a steep gradient at the edge and a good flat top in the center of the jet.

https://doi.org/10.1017/S0263034608000177 Published online by Cambridge University Press

Figure 3 shows the average energetic electron beam angular distribution in the forward laser direction, measured by RCF with the integration of 1640 laser shots together. It is seen that the average angular dispersion of the electron beam is less than 10°. Estimates based on the RCF sensitivity to the electron beam shows that the number of electrons in the 10° beam is approximately 2.4×10^9 electrons per shot. Assuming an average electron energy in the range of 1 to 5 MeV (dominated by a low energy continuum), the conversion efficiency to electrons with energies greater than 100 keV (the approximate detector cut-off energy) would be in the range of 0.2 to 1.0% (laser energy incident at the target was about 180 mJ for this series of shots). From the particle-in-cell (PIC) simulations, to be described later, an average electron temperature of the order of 1.4 MeV is observed for the bulk of the accelerated electrons.

Figures 4 and 5 show the typical electron energy spectra (horizontal axis) with one-dimensional (1D) spatial resolution (vertical axis) from both nitrogen and helium gases in the forward laser direction. For nitrogen alone and nitrogen mixed with 10% hydrogen, in most cases, one obtains multiple quasi-monoenergetic bunches with energies ranging from 12 MeV to 50 MeV, overlapped with a continuous energy spectrum as shown in Figures 4a and 4b. For helium, in most cases, multiple electron bunches with energy ranging from 25 MeV to 100 MeV could be observed to overlap with a weak continuous energy spectrum, as shown in Figures 5a and 5b. The continuous background electron distribution in the spectrum appeared weaker for helium than for nitrogen. Occasionally very bright energetic electron bunches were produced around 200 MeV, as shown in Figure 4c for nitrogen and Figure 5c for helium. Such exceptionally high energy shots, above 100 MeV, would occur on the order of less than 5% of the shots for nitrogen and on the order of about 40% of the shots for helium.

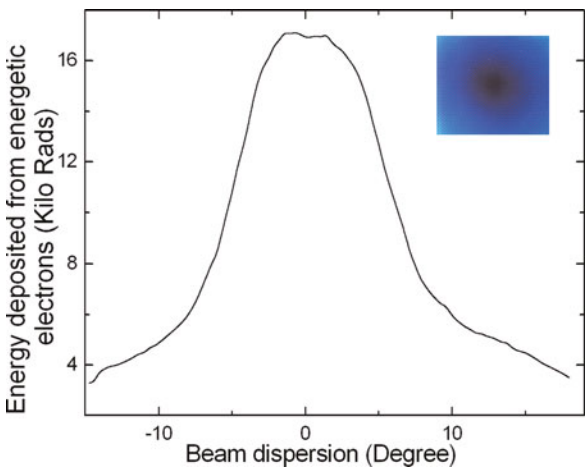

Fig. 3. (Color online) Energetic electron beam angular profile in the forward laser direction, integrated with 1640 shots when optimum conditions were adjusted to obtain mono-energetic electron beams. It was measured by RCF (inner frame) with nitrogen gas at about 360 psi and laser at the peak power. The laser beam forward direction is at 0°.

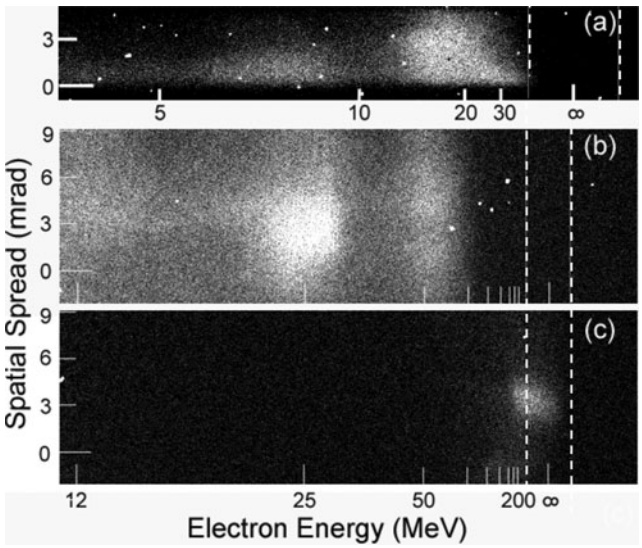

Fig. 4. Typical single-shot electron energy distributions generated from nitrogen gas targets, measured by Lanex fluorescent screen coupled to the electron spectrometer. Typical results are shown in (**a**) for pure N_2 at 500 psi backing pressure and (**b**) for N_2 with 10% H_2 at 360 psi. An example of an infrequent very high electron energy shot is shown in (**c**) for N_2 with 10% H_2 at 360 psi. The dashed lines show the location and width of the lead slit used to define the spectrometer entrance aperture.

The vertical angular spread of the electron bunches observed is on the order of 3 to 6 mrad as seen in Figures 4 and 5. This spread is much less than the average beam diameter of 10° observed from the radiochromic film as shown in Figure 3.

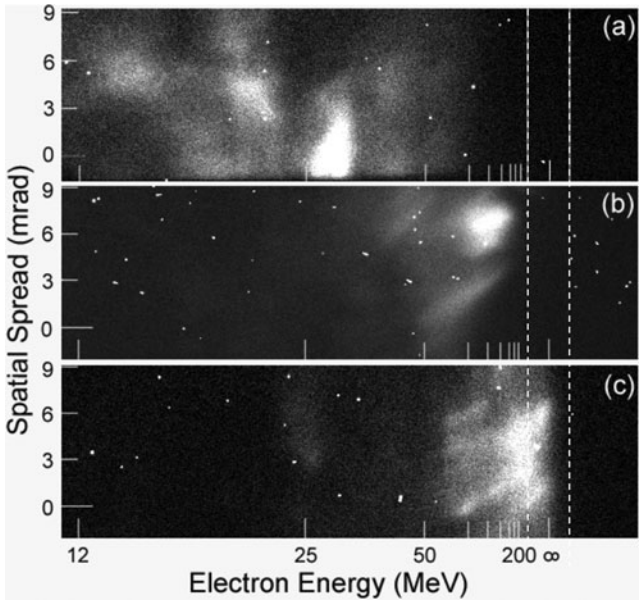

Fig. 5. Typical single-shot electron energy distributions generated from helium gas targets, measured by Lanex fluorescent screen coupled to the electron spectrometer. Typical results are shown in (**a**) and (**b**) for pure He at 900 psi backing pressure. An example of an infrequent very high electron energy shot is shown in (**c**) for He at 900 psi. The solid lines show the location and width of the lead slit used to define the spectrometer entrance aperture.

https://doi.org/10.1017/S0263034608000177 Published online by Cambridge University Press

The much broader beam diameter could correspond to a much broader background of continuum electrons observed as a background in Figures 4 and 5, which would also be dominated by lower energy electrons. The experiments show that the mono-energetic electron bunch generation from helium is somewhat more stable than that from nitrogen gas, especially when the laser is close to the peak power of 7 TW.

The corresponding electron energy spectra derived from the magnetic electron spectrometer observations given in Figures 4 and 5 are shown in Figure 6. Figures 6a and 6b show the two typical nitrogen spectra and helium spectra, respectively. Figure 6a shows that in most cases, the electrons from nitrogen gas are around 12 MeV to 50 MeV with several bunches overlapped on a continuous background.

For helium gas similar single shot spectra appear with peaks in the range of 25 to 100 MeV as shown in Figure 6b. When the electron energy spectra are averaged over many shots, a continuous quasi-Maxwellian distribution is observed. As shown in Figure 6c. The electron energy spectrum averaged over 20 shots from nitrogen gas shows a Maxwellian-like distribution, while for the helium gas jet, it shows a more plateau-like distribution with higher probability of generating energetic electron beams in energies ranging from 40 MeV to 140 MeV from the helium gas. These quasi-Maxwellian and plateau-like average energy distributions indicate that the more quasi-monoenergetic features observed on individual shots span a large range of energies with an exponentially decreasing probability of observing any one energy for nitrogen given by the temperature slope of the distribution function and with a more uniform probability of observing higher energy peaks for helium as observed above on individual shots. This is also in keeping with the low number of shots exhibiting very high energy peaks. In Figure 6d, the electron energy spectra from the exceptionally high energy single shots are given for nitrogen and helium gas. The

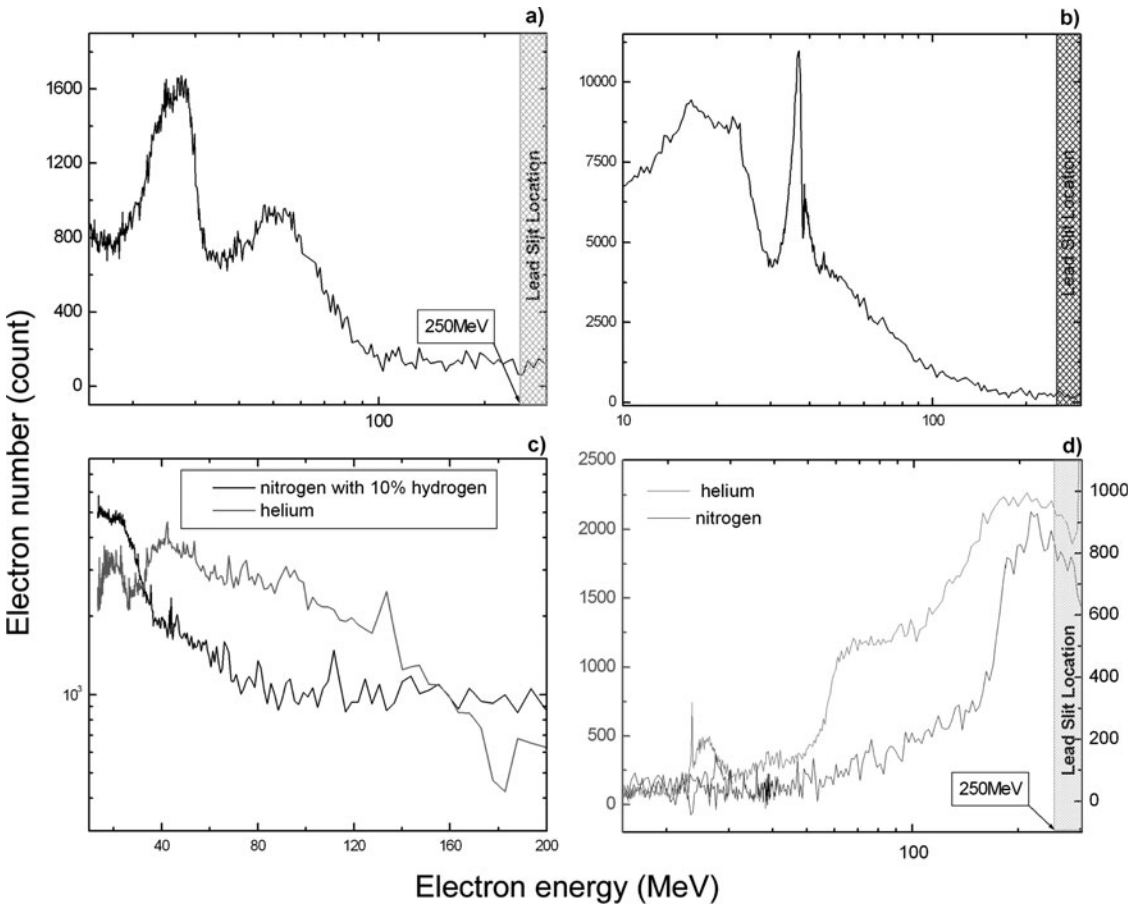

Fig. 6. Electron energy spectra obtained from the magnetic spectrometer images: **(a)** from a single shot in nitrogen with 10% hydrogen at 360 psi (Fig. 4b) integrated over 1.6 mrad of angular spread vertically, (**b**) from a single shot in helium at 900 psi (Fig. 5a) integrated over 10.6 mrad of angular spread vertically, (**c**) by averaging 26 shots from nitrogen gas with 10% hydrogen at 360 psi and 19 shots from helium gas at 900 psi, integrated over 19.2 mrad of angular spread vertically, and (**d**) energy spectra from the shots shown in Figures 4c and 5c showing the infrequent high energy electron bunches for nitrogen with 10% hydrogen and helium respectively integrated over 1.6 mrad of angular spread vertically. The scale in (**c**) is log-linear in order to allow visualization of the temperature slope while that on the other figures is linear-log to give better visualization of the relative widths of peaks. The response of the system has been calculated based on the camera response and fluorescence efficiency of the Lanex screen giving approximately one count generated in the image for each incident electron with energy from 10 MeV to 200 MeV.

https://doi.org/10.1017/S0263034608000177 Published online by Cambridge University Press

total energy generated in the quasi-monoenergetic bunches from helium appears to be approximately two times higher than that from nitrogen gas, which indicates a better energy conversion to the energetic electron beams from the helium gas. Estimate shows that the number of electrons in the mono-energetic electron beam recorded by the Lanex screen in the electron spectrometer is on the order of 10^6 each shot. This is a small fraction of the total number observed on the radiochromic film per shot. However, in this case, the energy per electron is much higher, typically on the order of 20 to 200 MeV, depending on the shot, and thus the total energy can still represent on the order of 2×10^{-5} to 2×10^{-4} of the incident energy. The radiochromic film views a much larger solid angle possibly integrating many such electron beamlets and also integrates all electron energies from 100 keV upward. For a quasi-Maxwellian electron energy spectrum, the majority of electron energies observed by the radiochromic film will be in the low end of the energy spectrum.

The prepulse level in the current experiments was on the order of 2×10^{-5} for the nanosecond leakage pulse, which arrives 8 ns prior to the main pulse and a picosecond pedestal at 5×10^{-5} of the main pulse intensity 1 ps prior to the peak of the main pulse and rising to 10^{-3} of the main pulse intensity at 0.4 ps prior to the main pulse. The effect of prepulse in enhancing the wakefield acceleration mechanism has already been pointed out by Giuletti *et al.* (2006, 2007) and Hosokai *et al.* (2006). Our experimental prepulse levels are not too different from those of Hosokai *et al.* (2006) where clear guide channels were observed formed by the prepulse. For nitrogen gas, this would be even more important due to the complex interaction of the femtosecond beam in ionizing the gas leading to filamentation, and defocusing in some cases as previously observed by Fedosejevs *et al.* (1997) and which also is complicated by ionization blue shifting of the leading edge of the laser pulse spectrum (Li & Fedosejevs, 1996). Thus, the preplasma formation may be required in order to stabilize the generation of quasi-monoenergetic electrons in nitrogen, explaining the lower energies and numbers of electrons observed on average in the electron bunches compared to helium gas. The requirement for the formation of a preplasma for nitrogen may also explain why the optimum density for MeV electron generation was quite high since higher densities would breakdown, absorb more energy from the laser prepulse, and form a channel with larger electron density gradients giving better guiding of the main pulse. Only rarely would a very long guide channel of just the right density conditions be formed at the right position for injection of the main beam to generate the 100 to 200 MeV electron bunches, which would explain the low frequency of observation of the very high energy electron bunches. Further experiments will be required in the future, using optical diagnostics, to better correlate the electron energies measured with the various preplasma conditions present.

The difference of the number of electrons measured by RCF and the Lanex fluorescent screen could be explained by a combination of the emission of multiple electron bunches in a given laser shot as well as a broad background of lower energy continuum electrons emitted in the forward direction. Noting the difference of the solid angle between RCF and Lanex, the 60 mm × 60 mm RCF was about 80 cm away from the target while Lanex was about 920 cm away with a 1 mm × 25 mm lead slit in the path about 355 mm from the target, as shown in Figure 1. The observation height on Lanex screen was only 18 mm, which is equivalent to 7 mm height on the slit. Thus only a small solid angle of the electron distribution function was observed by the Lanex screen in the electron spectrometer. Taking this solid angle difference gives a factor on the order of 100, which partially explains the ratio of the number of electrons measured by the two techniques. It is expected that more of the higher energy electrons, which require acceleration over longer propagation distances, will be in a small cone angle at the center of the distribution, and the lower energy electrons may be scattered over a larger cone angle. In addition, lower energy electrons (0.1–10 MeV) are not measured by the electron spectrometer but are still measured by the Radiochromic film. A larger number of such lower energy electrons may be produced by the interaction leading to the remaining factor of 10 larger Radiochromic film signal.

MODELING OF THE RESULTS

We have performed 2D (2D3V) PIC simulations with the relativistic multi-dimensional code MANDOR (Romanov *et al.*, 2004) in support of experiments. We have used parameters corresponding to the experimental conditions: the pulse has a Gaussian envelope with a FWHM diameter of 13 μm, a time duration at half maximum $\tau_L = 30$ fs, and a peak irradiation intensity 4×10^{18} W cm^{-2} ($a_0 = 1.4$, the normalized vector potential, $a_0 = eE_{pk}/mc\omega$, of the incident laser pulse). The ambient plasma electron density n_e is 5×10^{19} cm^{-3}, which corresponds to $n_e/n_c = 0.036$ with n_c being the critical density for the laser wavelength $\lambda_0 =$ 0.8 μm. The plasma is modeled as a homogeneous slab of density n_e with a 40 μm long ramp on the entrance surface where the density increases linearly. In this 2D simulation, we used 16 particles per cell in a 500 μm × 100 μm box (7500 × 1500 cells). Ions are considered immobile. For our conditions, the laser pulse length ($c\tau_L$~9 μm) is greater than the electron plasma wavelength $\lambda_p = 2\pi\ c/\omega_p$~4.2 μm or more accurately $\lambda_p = (2\pi\ c/\omega_p)\ (1 + (a_0)^2/2)^{1/4} = 5.4$ μm, if we account for the relativistic increase of an electron mass. Figure 7 shows the pulse intensity evolution as well as the 2D Fourier spectrum of the pulse at different locations inside the plasma. Figure 8 shows the formation of the electron density wake behind the propagating laser pulse at different times and Figure 9 shows the axial distribution of the electric fields and density profiles at two different times.

Initially, around 180 fs, when the pulse reaches the top of the ramp and enters into the homogeneous plasma, its shape is not modified, showing a total transverse size of around

https://doi.org/10.1017/S0263034608000177 Published online by Cambridge University Press

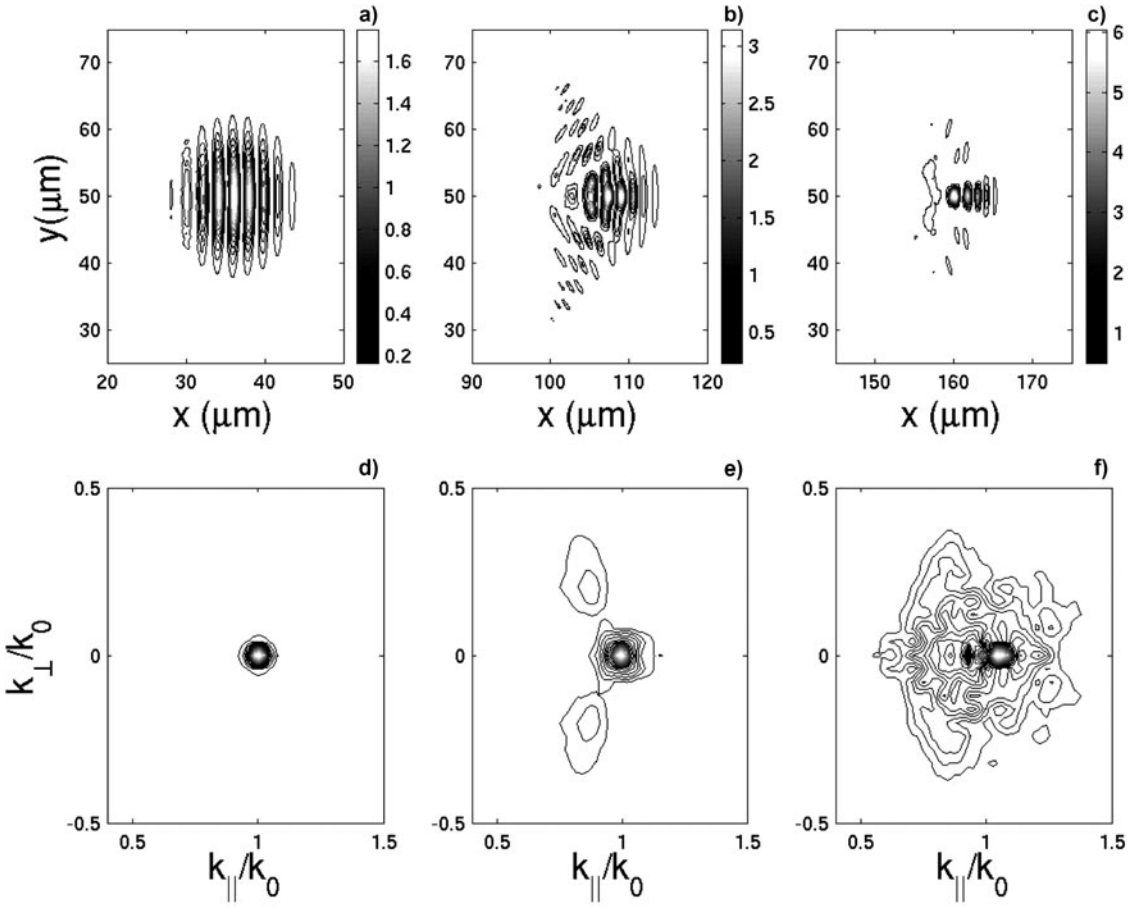

Fig. 7. Laser pulse from 2D3V PIC simulations at different time (**a**) t = 180 fs, (**b**) t = 425 fs, and (**c**) t = 606 fs, and 2D spectra of the laser pulse at the same times (**d**–**f**).

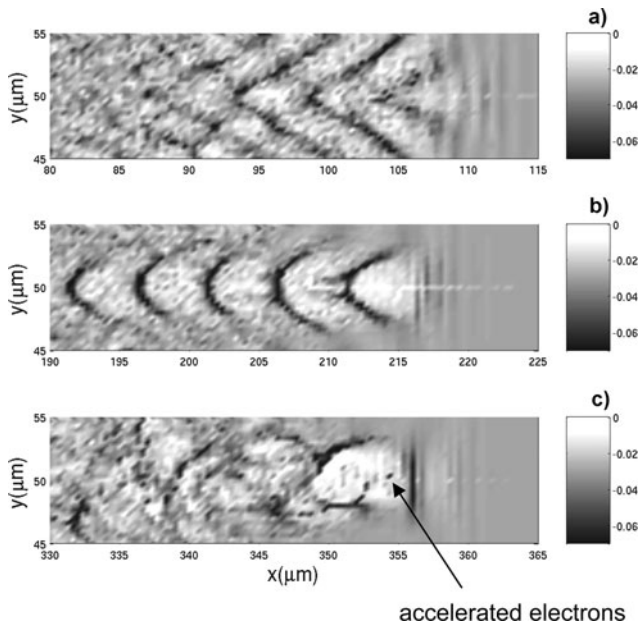

Fig. 8. Electron density (in units of n_c) for different times: (**a**) t = 425 fs, (**b**) t = 790 fs, and (**c**) t = 1273 fs.

20 μm and a longitudinal size of 18 μm (Fig. 7a). But as can be seen in Figure 7b, after 60 μm of propagation the laser pulse is modified by the stimulated Raman side-scattering instability, which can be identified by the presence of side-bands in the 2D spectrum (Fig. 7e). This forward-scattering leads to a decrease of light intensity in the focal region and contributes to a nonlinear pulse evolution which reduces the transverse size of the pulse. As shown in Figure 7b, after 60 μm of propagation the transverse size of the laser pulse is reduced by almost a factor two. In addition, in our case, the power is many times the critical power for relativistic self focusing, $P \sim 14 \times P_{crit}$ where $P_{crit} = 17\ GW \times n_e/n_c$ ($P_{crit} = 0.6$ TW for $\lambda = 800$ nm and $n_e = 5 \times 10^{19}\ cm^{-3}$). As illustrated in Figure 7f, the spectrum of the pulse is broadened along the transverse and longitudinal directions, which corresponds to the relativistic self-focusing. The effect of self-focusing corresponds also to the increase of a_0, by almost a factor three between the initial intensity and the maximum value observed during the simulation.

During the propagation through the plasma, the laser pulse is also strongly modified along the longitudinal direction. This behavior was already observed and discussed in

https://doi.org/10.1017/S0263034608000177 Published online by Cambridge University Press

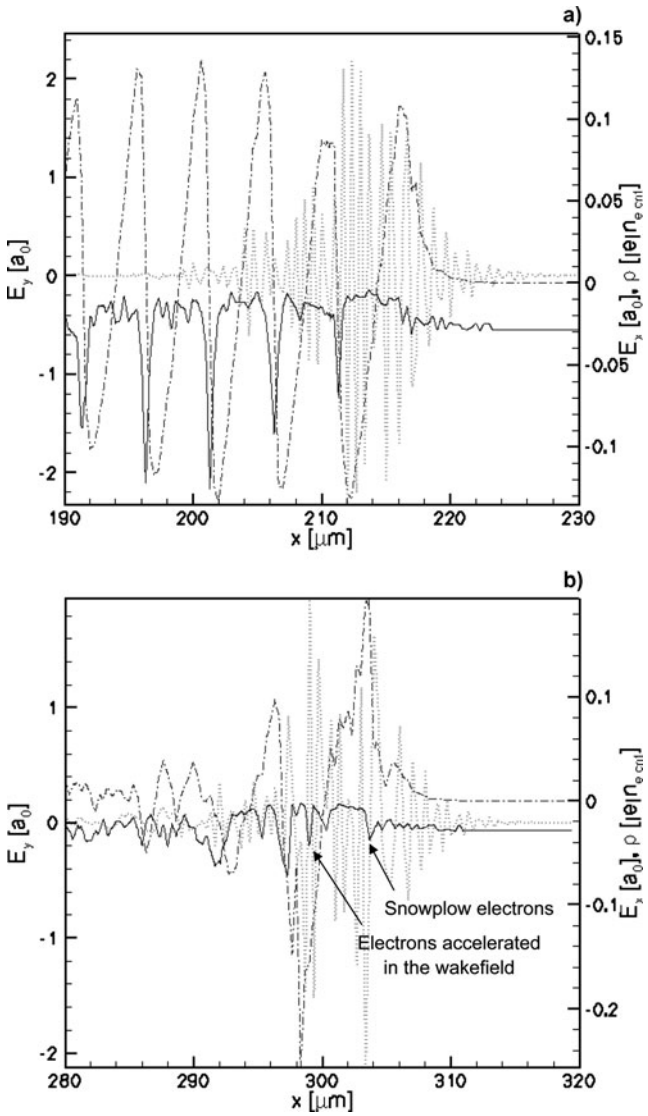

Fig. 9. Lineouts of the longitudinal field, E_x, (dash-dot), laser field, E_y, (dotted) normalized to $m\omega c/e$ and electron charge density (solid line) normalized to critical density along the x axis at two different times: (**a**) at $t = 849$ fs after propagating 180 microns in homogeneous plasma and (**b**) at $t = 1091$ fs when the wake is already broken and trapped-electrons are accelerated in the accelerating field. The ponderomotive force also accelerates electrons in front of the laser pulse (snowplow electrons).

previous simulations (Decker *et al.*, 1996). The front of the pulse is steepened because of group velocity dispersion (Decker *et al.*, 1996; Mori *et al.*, 1994), and it leads to pulse compression. At the same time the ponderomotive force of the leading edge accelerates electrons in front of the laser pulse leading to a density spike corresponding to accumulation of electrons due to a snowplow effect. The front of the pulse experiences a frequency downshift or a photon deceleration (Tsung *et al.*, 2002) due to the resultant gradient in index of refraction. The laser energy decreases while the photon number density is conserved therefore the front of the pulse experiences a frequency downshift (photon deceleration) as can be seen in Figure 9b.

Figure 7f shows the 2D spectrum of the pulse after 120 μm of propagation in the homogeneous density plateau, the part of the spectrum of the laser is strongly downshifted to low value of k. As a result, we observe a shortening of the pulse as shown in Figure 7c, where the length of the pulse is reduced by more than a factor of three. Shortening of a laser pulse during the propagation in an underdense plasma has already been measured in previous experiments (Faure *et al.*, 2005) and attributed to a broadening of the laser spectrum due to relativistic self-phase modulation (Wilks *et al.*, 1989).

During the propagation of the pulse inside the plasma, a regular plasma wave is created (Fig. 8b) with a wavelength of almost 5 μm close to the estimated value with the relativistic corrections. These waves are curved due to the transverse wave breaking (Bulanov *et al.*, 1997). Between each wave, we observe a cavity, which contains a number of electrons (Figs. 8c and 9a). A number of electrons are localized in a small spike in the front of the laser pulse (Fig. 8c, represented by a small black streak). After 300 μm of propagation in the homogeneous density, the wave breaks and a number of trapped electrons are accelerated in the accelerating part of longitudinal field inside the first cavity (Fig. 9b). This breaking occurs for a maximum value of the longitudinal field E_x of almost 0.15 E_0 (with $E_0 = \omega_0 mc/e$), which is lower than the relativistic expression for the wave breaking (in the cold plasma approximation), given by $[2(\gamma_{ph}-1)]^{1/2}(\omega_{pe}/\omega_0)E_0$ (Arkhiezer & Polovin, 1956), which in our case, is around $0.5E_0$, where γ_{ph} is the Lorentz factor associated with the plasma wave phase velocity, which for very underdense plasma is almost $(n_c/n_e)^{1/2}$. The energy spectrum of these electrons inside this cavity is illustrated in Figure 10. Just after the wave breaking, the energy spectrum shows two bunches of electrons with energies around 10 MeV

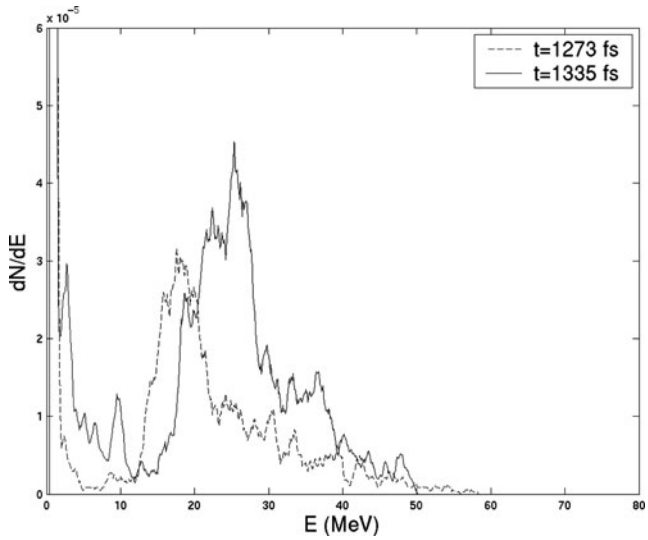

Fig. 10. Energy spectrum of electrons inside the first cavity for two different times: 1273 fs and 1335 fs.

https://doi.org/10.1017/S0263034608000177 Published online by Cambridge University Press

and 20 MeV and finally it evolves to form only one peak around 30 MeV, close to the experimental results.

The occasional electrons generated at 200 MeV are probably generated by the so-called mechanisms of the "bubble" acceleration (Mangles *et al.*, 2004; Geddes *et al.*, 2004; Faure *et al.*, 2004), which is a wakefield acceleration in the highly nonlinear wave breaking regime. Several conditions are necessary for this mechanism. In particular, the transverse and longitudinal dimensions of the laser pulse must be not far from half of the plasma wavelength in order to be able to create this cavity (the bubble), void of electrons. A similarity theory recently introduced (Gordienko & Polovin, 2005) gives a threshold for the power of the pulse in order to create this cavity: $P > P_{bubble} = [\tau(fs) \ / \ \lambda(\mu m)]^2 \times 30GW$. In our case, we are initially well below this threshold. Nevertheless, it has been observed recently (Hidding *et al.*, 2006) that a long pulse which didn't fulfill this conditions, can evolve into a pulse which finally matches this threshold because of a shortening of its duration due to the self-modulation, leading to the observation of monoenergetic electron bunches. In our set of simulations, we observed the same evolution of the pulse, where at the end, its longitudinal size is reduced by more than a factor of three, as shown in Figure 7c. Such a reduction of pulse duration down to approximately 10 fs reduces the required power to $P_{bubble} = 4.7$ TW. At the same time the pulse compression leads to the peak pulse power of 1.3 TW. Thus the interaction would not approach the full bubble regime in our simulations at the full background gas density. Thus, different starting conditions, such as a reduced density channel from a prepulse would be required in order to enter this regime.

Our modeling here is only 2D and it is well known that often 2D simulations underestimate the maximum electron energy (Tsung *et al.*, 2006), and fail to describe the self focusing correctly, even if the physics and the interaction is correctly described. This self focusing could lead to higher local laser intensities helping in the creation of bubble structures and leading to the generation of the higher laser energies.

In the present case, there is another important factor limiting the maximum electron energy which can be generated. The high density in the present experiments would lead to very short interaction lengths due to the rapid dephasing of the electron bunch and the laser wakefield. The standard scaling laws for wakefield acceleration (Mangles *et al.*, 2004) indicate that high energy electron production requires long interaction lengths at lower densities. Such long low density interaction lengths may occasionally be present in our experiment with the existence of a preplasma formed low density channel. The effect of preplasma created channels has already been reported in the literature (Hosokai *et al.*, 2006; Giulietti *et al.*, 2006), where a plasma cavity was formed by the prepulse picoseconds earlier than the main pulse. The main pulse was then guided by this cavity and formed a plasma channel, which significantly improved the generation of mono-energetic electrons. Our prepulse levels are similar to those reported by Hosokai *et al.* (2006) in their low prepulse case and thus we might expect similar conditions. The variability of the prepulse from shot to shot and the exacting conditions for the injection of the main pulse into such a channel would explain why only very few shots produce the high, 200 MeV, energy electrons occasionally observed.

In terms of the number of electrons observed in the PIC simulations, the energy contained in the 20 to 30 MeV bunch shown in Figure 10 is 1.4 μJ corresponding to 334,000 electrons. This is comparable to the number of electrons observed per electron bunch electron in the experiments of approximately 10^6. Also, in the simulation almost all of the high energy electrons were accelerated in a cone angle of 20°. This is in approximate agreement with the observed cone angle of 10° (FWHM) for the electrons observed from the radiochromic film in the experiments. Thus, the overall number of electrons generated in the quasi-monoenergetic bunches and the overall directionality is in qualitative agreement with the experiment.

CONCLUSION

In conclusion, experiments show that quasi-monoenergetic electron beams with energies on the order of 10 to 50 MeV are generated in nitrogen and of energies of 25 to 100 MeV in helium for 7 TW laser pulses incident into plasma electron densities of $10^{20}\,cm^{-3}$ and $5 \times 10^{19}\,cm^{-3}$, respectively. Occasionally electrons with energy over 200 MeV can be generated from laser pulses interacting with both nitrogen and helium gases. These very high energy electrons are most likely associated with the occasional occurrence of optimum preformed guide channels in the plasma due to the nanosecond and picosecond prepulse. The average energy distribution functions, which to some extent represent probability distribution function for the monoenergetic peaks versus energy, are quasi-Maxwellian for nitrogen gas and more plateau-like up to 140 MeV for helium gas. These are in keeping with the low number of shots observed with very high energy peaks above 150 MeV. Overall 2.5×10^9 electrons per shot were recorded in a cone angle of 10° (FWHM), while 10^6 electrons are generated in the quasi-monoenergetic bunches. 2D PIC simulations of the interaction of the laser pulse with plasma at an electron density of $5 \times 10^{19}\,cm^{-3}$ indicates the production of a 20–30 MeV electron energy electrons consistent with majority of the shots in the experiment. During the interaction, the pulse evolves through Raman scattering, self phase modulation and self focusing leading to a shortening and increase in intensity. This allows the pulse to approach the threshold for the bubble regime as required for high energy electron acceleration. However, lower densities and longer interaction lengths would be required for the acceleration of electrons to very high energies of 200 MeV, which would depend on the formation of a preplasma in the experiment. Further

https://doi.org/10.1017/S0263034608000177 Published online by Cambridge University Press

experiments will be carried out in the future to better correlate the resultant electron energies with the various plasma conditions present using optical diagnostics to monitor the preplasma formation. In the present experiments and simulations, a better understanding of the conditions required for quasi-monoenergetic electron pulses has been obtained and the possibility of controlling the generation of higher energy electrons through the use of optimum prepulses will be explored in the future.

ACKNOWLEDGMENT

The authors would like to thank the technical staff of ALLS for their expert technical support and help in this project. The authors would also like to acknowledge funding for this work from the Natural Sciences and Engineering Research Council and thank the Canadian Institute for Photonic Innovations for providing travel funds for one of the researchers (ZLC).

REFERENCES

Arkhiezer, A.I. & Polovin, R.V. (1956). Theory of wave motion of an electron plasma. *Sov. Phys. JETP* **3**, 696.

Bulanov, S.V., Pegoraro, F., Pukhov, A.M. & Sakharov, A.S. (1997). Transverse-wake wave breaking. *Phys. Rev. Lett*. **78**, 22.

Decker, C.D., Mori, W.B., Tzeng, K.-C. & Katsouleas, T. (1996). The evolution of ultra-intense, short-pulse lasers in underdense plasmas. *Phys. Plasmas* **3**, 2047.

Faure, J., Glinec, Y., Pukhov, A., Kiselev, S., Gordienko, S., Lefebvre, E., Rousseau, J.-P., Burgy, F. & Malka, V. (2004). A laser-plasma accelerator producing monoenergetic electron beams. *Nature* **431**, 541.

Faure, J., Glinec, Y., Santos, J.J., Ewald, F., Rousseau, J.-P., Kiselev, S., Pukhov, A., Hosokai, T. & Malka, V. (2005). Observation of laser-pulse shortening in nonlinear plasma waves. *Phys. Rev. Lett*. **95**, 205003.

Fedosejevs, R., Wang, X.F. & Tsakiris, G.D. (1997). Onset of relativistic self-focusing in high density gas jet targets. *Phys. Rev. E* **56**, 4615.

Geddes, C.G.R., Toth, CS., Tilborg, J.VAN, Esarey, E., Schroeder, C.B., Bruhwiler, D., Nieter, C., Cary, J., & Leemans, W.P. (2004). High quality electron beams from a laser wakefield accelerator using plasma-channel guiding. *Nature* **431**, 538.

Giulietti, A., Tomassini, P., Galimberti, M., Guilietti, D., Gizzi, L.A., Koester, P., Labate, L., Ceccotti, T., D'oliveira, P., Auguste, T., Monot, P. & Martin, P. (2006). Prepulse effect on intense femtosecond laser pulse propagation in gas. *Phys. Plasmas* **13**, 093103.

Giulietti, A., Galimberti, M., Gamucci, A., Guilietti, D., Gizzi, L.A., Koester, P., Labate, L., Tomassini, P., Ceccotti, T., D'oliveira, P., Auguste, T., Monot, P. & Martin, P. (2007). Search for stable propagation of intense femtosecond laser pulses in gas. *Laser and Particle Beams* **25**, 513.

Gordienko, S. & Pukhov, A. (2005). Scalings for ultrarelativistic laser plasmas and quasimonoenergetic electrons. *Phys. Plasmas* **12**, 043109.

Hidding, B., Amthor, K.-U., Liesfeld, B., Schwoerer, H., Karsch, S., Geissler, M., Veisz, L., Schmid, K., Gallacher, J.G., Jamison, S.P., Jaroszynski, D., Pretzler, G., & Sauerbrey, R. (2006). Generation of quasimonoenergetic electron bunches with 80-fs laser pulses. *Phys. Rev. Lett*. **96**, 105004.

Hosokai, T., Kinoshita, K., Ohkubo, T., Maekawa, A., Uesaka, M., Zhidkov, A., Yamazaki, A., Kotaki, H., Kando, M., Nakajima, K., Bulanov, S.V., Tomassini, P., Giulietti, A. & Guilietti, D. (2006). Observation of strong correlation between quasimonoenergetic electron beam generation by laser wakefield and laser guiding inside a preplasma cavity. *Phys. Rev. E* **73**, 036407.

Hsieh, C.-T., Huang, C.-M., Chang, C.-L., Ho, Y.-C., Chen, Y.-S., Lin, J.-Y., Wang, J. & Chen, S.-Y. (2006). Tomography of injection and acceleration of monoenergetic electrons in a laser-wakefield accelerator. *Phys. Rev. Lett*. **96**, 095001.

Leemans, W.P., Nagler, B., Gonsalves, A.J., Toth, CS., Nakamura, K., Geddes, C.G., Esarey, R.E., Schroeder, C.B. & Hooker, S.M. (2006). GeV electron beams from a centimeter-scale accelerator. *Nature Physics* **2**, 696.

Li, Y.M. & Fedosejevs, R. (1996). Ionization-induced blue shift of KrF laser pulses in an underdense plasma. *Phys. Rev. E* **54**, 2166.

Lifschitz, A.F., Faure, J., Malka, V. & Mora, P. (2005). GeV wakefield acceleration of low energy electron bunches using petawatt lasers. *Phys. Plasmas* **12**, 093104.

Lifschitz, A.F., Faure, J., Glinec, Y., Malka, V. & Mora, P. (2006). Proposed scheme for compact GeV laser plasma accelerator. *Laser and Particle Beams* **24**, 255.

Mangles, S.P.D., Murphy, C.D., Najmudin, Z., Thomas, A.G.R., Collier, J.L., Dangor, A.E., Divall, E.J., Foster, P.S., Gallacher, J.G., Hooker, C.J., Jaroszynski, D.A., Langley, A.J., Mori, W.B., Norreys, P.A., Tsung, F.S., Viskup, R., Walton, B.R. & Krushelnick, K. (2004). Monoenergetic beams of relativistic electrons from intense laser-plasma interactions. *Nature* **431**, 535.

Mori, W.B., Decker, C.D. & Katsouleas, T. (1994). Particle-in-cell simulations of Raman forward scattering from short-pulse high-intensity lasers. *Phys. Rev. E* **50**, R3338.

Ozaki, T., Kieffer, J.-C., Toth, R., Fourmaux, S., & Bandulet, H. (2006). Experimental prospects at the Canadian advanced laser light source facility. *Laser and Particle Beams*. **24**, 101.

Romannov, D.V., Bychenkov, V.YU., Rozmus, W., Capjack, C.E., & Fedosejevs, R. (2004). Self-organization of a plasma due to 3D evolution of the Weibel instability. *Phys. Rev. Lett*. **93**, 215004.

Tajima, T. & Dawson, J.M. (1979). Laser electron accelerator. *Phys. Rev. Lett*. **43**, 267.

Tsung, F.S., Ren, C., Silva, L.O., Mori, W.B. & Katsouleas, T. (2002). Generation of ultra-intense single-cycle laser pulses by using photo deceleration. *Proc. Natl. Acad. Sci. U.S.A* **99**, 29.

Tsung, F.S., Lu, W., Tzoufrsa, M., Mori, W.B., Joshi, C., Vieira, J.M., Silva, L.O. & Fonseca, R.A. (2006). Simulation of monoenergetic electron generation via laser wakefield accelerators for 5–25 TW lasers. *Phys. Plasmas* **13**, 056708.

Wilks, S.C., Dawson, J.M., Mori, W.B., Katsouleas, T. & Jones, M.E. (1989). Photon accelerator. *Phys. Rev. Lett*. **62**, 2600.